Flow Measurement and Instrumentation 21 (2010) 255–261

Contents lists available at ScienceDirect

Flow Measurement and Instrumentation

journal homepage: www.elsevier.com/locate/flowmeasinst

Advanced three-dimensional multiphase flow simulation in porous media reconstructed from X-ray Microtomography using the He–Chen–Zhang Lattice Boltzmann Model

C.L. Lin, A.R. Videla, J.D. Miller *

Department of Metallurgical Engineering, College of Mines and Earth Sciences, University of Utah, 135 South 1460 E. Room 412, Salt Lake City, UT 84112, USA

ARTICLE INFO

Article history:
Received 16 June 2009
Received in revised form
20 January 2010
Accepted 22 February 2010

Keywords:
Multiphase flow simulation
LBM
Porous media
X-ray microtomography

ABSTRACT

Multiphase flow is a subject of significant interest in the processing of mineral resources and to processing industries in general. Multiphase flow is of significance in the transport of reactants during the percolation of leaching solution in heaps, in the melting of metals, in phase transformation, metal foam processes, underground water transport, in gas and oil recovery and in gas sequestration, just to mention a few examples.

The lattice Boltzmann model (LBM) of multiphase fluid flow has now become a collection of models with varying degrees of faithfulness to the properties of real fluids. These models are in a state of evolution as they are becoming better understood and are extended to new applications. In this paper we address the application of a single-component multiphase flow LBM known as the He–Chen–Zhang model coupled with X-ray microtomography (XMT) for the digitalization and simulation of flow in porous media. The model is used for the simulation of fluid penetration into porous samples and the analysis of capillary phenomena. Specifically, this model has been applied for the simulation of percolation in a packed bed of sand particles which is digitalized by XMT.

1. Introduction

The numerical simulation of multiphase flow is a challenging subject because the simulation requires tracking in time of the interfaces between the different fluids. The standard approaches used by the computer fluid dynamics community have included the free-boundary methods (for example, that of Zhang and Stone [1]), and the numerical-diffuse-interface methods such as front-tracking (FT) and front-capturing (FC) methods [2,3]. Even though these methods have shown success in simulation of some problems they still fail when the multiphase fluid involves strong changes of morphology and topology as in the case of multiphase flow in complex pore geometries.

Unlike traditional computational fluid dynamics (CFD) methods which resolve macroscopic governing equations, the LBM simulates fluid flow based on microscopic and mesoscopic models. The LBM microscopic model allows for the incorporation of many physics phenomena related to the mesoscopic length scale, some of which are essential to approximate the complex problems of interest. In fact, the intermolecular interactions which account for the interfacial dynamics are naturally incorporated into the model due to their mesoscopic scale. The microscopic interaction forces are incorporated into the lattice Boltzmann equation in such a way as to mimic the interactions governing the interface dynamics.

The LBM of multiphase flow dynamics has now become a collection of models with varying degrees of faithfulness to the properties of real fluids. These models are in a state of evolution as the models are becoming better understood. In fact, as some of their deficiencies are corrected new challenges are also found.

1.1. Physics of multiphase flow in porous media

The flow of two immiscible fluids simultaneously sharing the complex pore space in a porous medium is governed by the forces acting on the fluids, including pressure forces, viscous forces, gravity forces, inertia forces and interfacial surface forces. The relative importance of these forces is usually characterized by the Reynolds (Re), bond (Bo), and capillary (Ca) numbers, and the viscosity ratio (M). In general, flow in porous media is dominated by the capillary forces, where inertia forces are negligible, and the pressure forces and viscous forces are proportional to the rate of flow. Because the inertia forces and pressure forces depend on the flow rate, the capillary forces and gravitational forces become more important when the rate of flow is slower.

* Corresponding author. Tel.: +1 801 581 5160; fax: +1 801 581 4937.
E-mail addresses: chenluh.lin@utah.edu (C.L. Lin), Jan.Miller@utah.edu (J.D. Miller).

0955-5986/$ – see front matter © 2010 Elsevier Ltd. All rights reserved.
doi:10.1016/j.flowmeasinst.2010.02.008

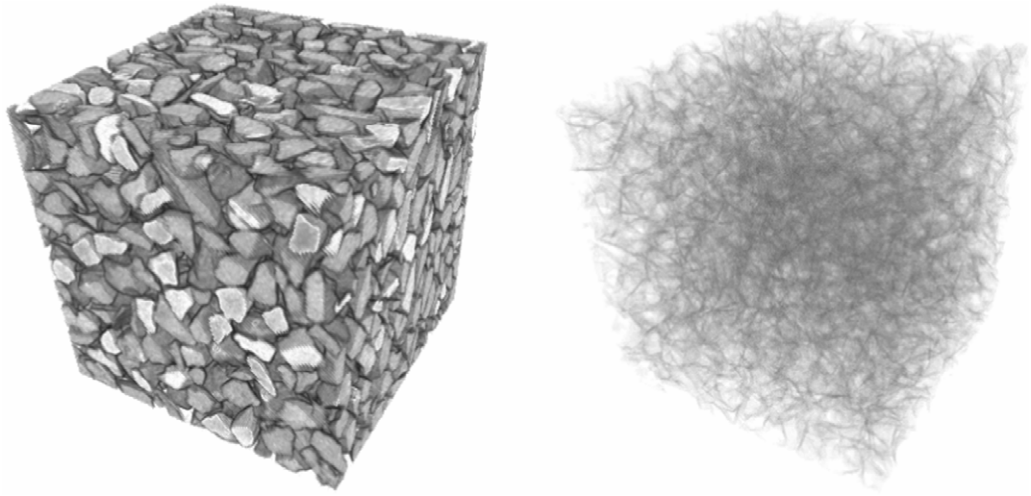

Fig. 1. 3D image reconstruction of a packed bed of sand particles (300 × 425 μm). The voxel resolution is 20 μm and the image size contains 200 × 200 × 200 voxels. The left-hand side image shows the packed particle bed and the right-hand side image shows the porous network structure.

Interfacial shapes in static and quasi-static situations are governed by the Laplace equation. By applying the condition of mechanical equilibrium of the forces acting on the interface, Laplace showed that the capillary pressure is proportional to the interfacial tension and inversely proportional to the curvature of the meniscus. The Laplace law is shown in Eq. (1) for a three-dimensional (3D) pore structure; it is dependent on the interfacial tension γ_{12} and the radius of curvature, r^*.

$$p_2 - p_1 = p_c = 2\frac{\gamma_{12}}{r^*}, \quad \text{with } \frac{1}{r^*} = \frac{1}{2}\left(\frac{1}{r'} + \frac{1}{r''}\right). \tag{1}$$

Porous structures involve the presence of a solid phase which in a capillary system interacts with at least two fluid phases. As a result there are at least three surfaces subjected to surface tension. The static equilibrium between the three interfacial tensions leads to the well-known Young's equation, as shown in Eq. (2).

$$\gamma_{lg}\cos\theta = \gamma_{sg} - \gamma_{sl}. \tag{2}$$

The contact angle is normally used to describe the preferential characteristics of the solid surface to be wet. In some cases, no equilibrium is possible $\left(\gamma_{lg} > \gamma_{sg} - \gamma_{sl}\right)$ and the liquid covers the whole surface completely; in such cases the liquid is said to wet the solid perfectly.

2. X-ray microcomputed tomography (XMT)

X-ray tomographic imaging is, in general terms, an X-ray-based method which by radiation of an opaque sample in different directions allows its 3D reconstruction. The development of this non-invasive technique is recent, but it has had a huge impact in several areas of science. In fact, the first device capable of producing true reconstructed images was developed by Hounsfield as recently as 1972 at EMI in England, and it was based, in part, on mathematical methods developed by Cormarck a decade earlier [4].

The mechanics of X-ray tomography testing is relatively simple. The sample is located between the X-ray source and the detector. Then the sample is illuminated in different directions, and for each direction the projection of the attenuation coefficients is measured. Finally, a computerized reconstruction is carried out. The reconstruction of the samples is based on a mathematical formalism known as the Radon transform and its mathematical framework. After processing, the CT produces a spatial description of the object under analysis where the field of view is divided into elemental digital units known as voxels. Each voxel is characterized by the attenuation coefficient of the material inside it. This spatial digital characterization of the sample under analysis allows for further digital processing of the sample.

Fig. 1 shows a packed bed of sand particles and its porous network structure as obtained by the micro CT system. The particle size is between 300 and 425 μm, the resolution of each voxel is 20 μm in length and the size of the image is 200 × 200 × 200 voxels. It is possible to observe how image processing of the digital data allows a clear separation between the solid and the air due to the clear difference in attenuation coefficients. This technique easily obtains the porous network of the packed particle bed by filtering and thresholding. During simulation, the fluid flows through this network structure having a specific connectivity with well-defined pore dimensions not only to determine the local flow but also the overall permeability of the sample.

The separation of the particles and the air in the 3D image is a fairly simple process given the high contrast between the attenuation coefficients of both elements. During the separation process, first the noise of the intensity image obtained from the X-ray CT scan is reduced by using a linear spatial filter which replaces the intensity of each voxel by the average of the intensity values of the voxel itself and the intensity of a defined neighborhood region; for example, a mean filter is usually applied with a 3 × 3 × 3 kernel. After filtering, the image is segmented into only two elements by using the histogram of the intensities which can usually be interpreted as a bi-modal distribution between the air and the particles. The threshold process consists in the determination of the best thresholding value to separate the two modes (particles and air) from each other. In this way, the thresholding process converts an intensity image composed of several attenuation coefficient values into a black and white binary image. The resulting image will define the pore network structure used for simulations, as shown in Fig. 1.

The images of porous structures for packed particle beds reveals why the LBM method is more suitable for this kind of problem than the standard CFD mesh methods. The standard solution with a CFD solver requires the construction of a grid, the definition of the boundary conditions in the boundary nodes, and the solution of the Navier–Stokes equation at each node. The standard CFD methodology, therefore, will require an enormous amount of time for grid construction and also for computer simulation.

3. Lattice Boltzmann model and simulation of fluid flow through porous media

3.1. The single-component multiphase He–Chen–Zhang model

Several lattice Boltzmann multiphase fluid flow models have been introduced in the past years finding applications in different areas of fluid dynamics such as phase separation [5], fingering phenomena in a channel [6,7], and metal foam [8] among others. The major advantage claimed for pursuing the use of LBM instead of standard CFD methods resides in its ability to model complex solid boundaries in any arbitrary geometry, a scheme suitable for code parallelization, and ability to incorporate microscopic force interactions that control the interface dynamics.

In general, the LBM of multiphase flow can be described as single-component or multicomponent models. Single-component models describe phase separation by an equation of state that under the critical temperature automatically segregates phases into two stable densities, vapor (light density) and liquid (heavy density). In this category we found the single-component Shan and Chen model [9–12], single-component free-energy model and the He–Shan–Doolen model to be of interest. On the other hand, multicomponent models use one particle distribution function (PDF) and one evolution equation to represent each fluid component in the system, and segregation is simulated by interaction between the two independent fluids. The Shan and Chen model and the free-energy model [13,14] also have multicomponent versions, and, additionally, in this category is found the chromodynamic model [15–17]. For further discussion and comparison of all these methods the reader is referred to the work done by Chen and Doolen [18], Do-Quang et al. [19], He and Doolen [20], Hazi et al. [21] and Nourgaliev et al. [22].

We start with the description of the single-component multiphase flow due to He, Chen and Zhang. In their seminal work, He et al. [23,24] present a new multiphase model derived directly from discretizing the continuous kinetic equation for non-ideal fluids modified for incompressible flow. As was mentioned previously, the He–Chen–Zhang [23] model is an extension of the He–Shan–Doolen model [25]. The model has not being used extensively and is not as popular as the Shan and Chen model. The authors have applied the model to two 2D and 3D Rayleigh–Taylor instability simulations [23,24,26] and compared the data with theoretical values and another CFD simulation showing good qualitative and quantitative results. More recently, Lee and Lin [27] have extended the model to simulate the evolution of a droplet splashing on a thin film.

Unlike the traditional CFD methods that resolve the macroscopic governing equations using a free boundary surface approximation, the He–Chen–Zhang model simulates the interfacial dynamics, such as phase segregation and surface tension, from mesoscopic kinetic equations. In this model the interfacial dynamics is the result of molecular interactions where two distributions functions are used, one for tracking the pressure and velocity, and another for tracking only the density. When the molecular attraction is strong enough, the fluid automatically segregates into two different phases. One of the major advantages with respect to the Shan and Chen model is that the surface tension in the He–Chen–Zhang model can be adjusted beforehand by a free parameter due to its consistent thermodynamic.

Theoretically speaking, the use of these equations of state could allow reaching high density ratios for the saturated fluid density. The problem arising is that as the density ratios increase the spurious velocity magnitudes also increase, making the simulations numerically unstable. We have been able to run simulations with density ratios up to 30. Numerical instability is an area that requires more research in the whole subject of the LBM.

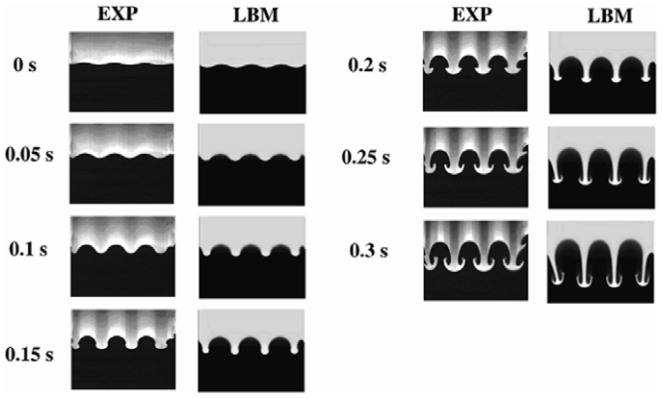

Fig. 2. Qualitative comparison of experiments and simulations for the Rayleigh–Taylor instability phenomena.

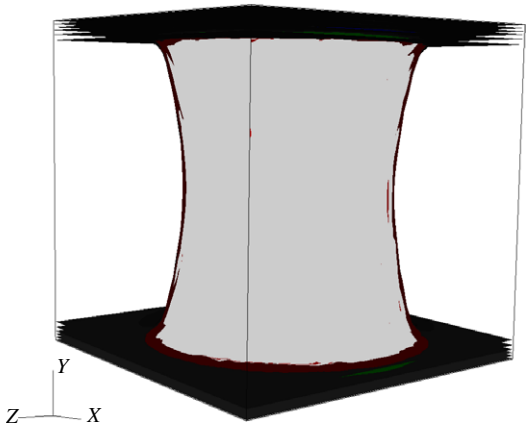

Fig. 3. Simulated 3D image of fluids in contact with the solid. Conditions: contact angle 45 degrees ($D_\rho = 0.5$) and $\rho_l/\rho_g = 10$.

3.2. Rayleigh–Taylor instability—verification

In the LBM community there is a lack of comparison of simulation data with experimental data. Recently Waddell et al. [28] have published experimental results where the Rayleigh–Taylor instability is observed by using planar laser-induced fluorescence and recorded using a video camera attached to a tank which travels vertically on a linear rail system. A weight and pulley system is used to accelerate downwards the two fluids in the tank in excess of the earth's gravitational acceleration and driving the fluid flow.

Fig. 2 shows a sequence of images where in the left column are the experimental images published in Waddell et al. and in the right column are the result of simulations using our implementation of the He–Chen–Zhang model. In the experiment the Atwood number is 0.336 and the Reynolds number is approximately 3000. The 121 mm wide tank was accelerated at $0.32g$ with an initial perturbation of 35 mm. The surface tension of the fluid mixture was very small. The first frame of the experiment shows the system slightly after release and then each frame is at 0.05 s increments.

As is shown in Fig. 2, the LBM shows a very close behavior to the experiments where all the main structures such as the different spikes and roll ups are present. It is impressive to observe that the spikes located right beside the edges of the container also shown the same inclinations due to the boundary conditions. Even though there is good agreement in the general flow configurations, the simulation shows differences in the length and size of the mushroom shapes. Improvement of these results may require more care in the settings of the simulation, like fluid viscosities

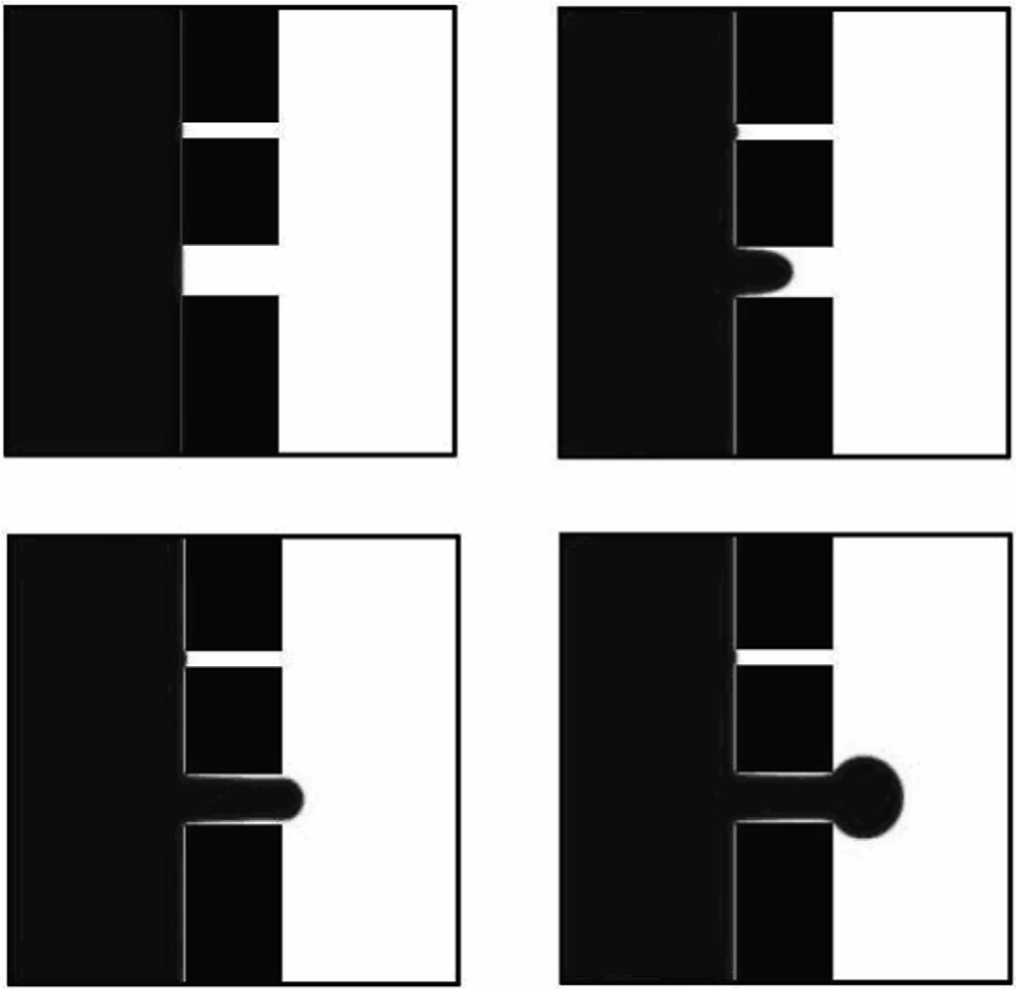

Fig. 4. Simulations of fluid displacement in a capillary tube with two throats of different radius. From left to right and top to bottom image: flow after 1000, 10 000, 20 000 and 30 000 iterations. A D2Q9 lattice of size 35 × 130 lu^2 was used. The parameters for simulations are $\bar{k} = 0.1$, $D = 0.99$ and $\rho_l/\rho_g = 10$.

and surface tension. The comparison between the experiments and the simulation results shows qualitatively that the model describes the physics of the complex Rayleigh–Taylor problem correctly, and therefore a good qualitative description of interface motion in other problems can be expected.

3.3. Wettability

The original model proposed by He et al. [23] does not account for solid–fluid interactions. In order to include solid–fluid interaction at the solid–fluid interface we use a similar mathematical artifact to the one proposed in the model of Rothman and Zaleski [29] and recently Yiotis et al. [30]. In doing so, the affinity of the solid to the fluid phases is controlled by the density of the solid node. A density of the solid near to the density of the heavy fluid will in fact attract the heavy fluid to the solid surface, and in contrast, a density of the solid near the density of the light fluid will attract the light fluid to the solid surface through the external force included in the evolution model. Results show a linear relationship between the contact angle and the solid density. Fig. 3 shows the resulting contact angle at static equilibrium for different values of the solid density as a function of the parameter D_ρ, as defined in Eq. (3).

$$D_\rho = \frac{\rho_{solid} - \rho_g}{\rho_l - \rho_g}. \tag{3}$$

Fig. 3 shows the contact angle formed when two fluids are set between two walls in 3D simulation. As the parameter D_ρ is close to zero, meaning that the solid density is close to the gas density, the solid presents an affinity for the light fluid (black color in Fig. 3). In

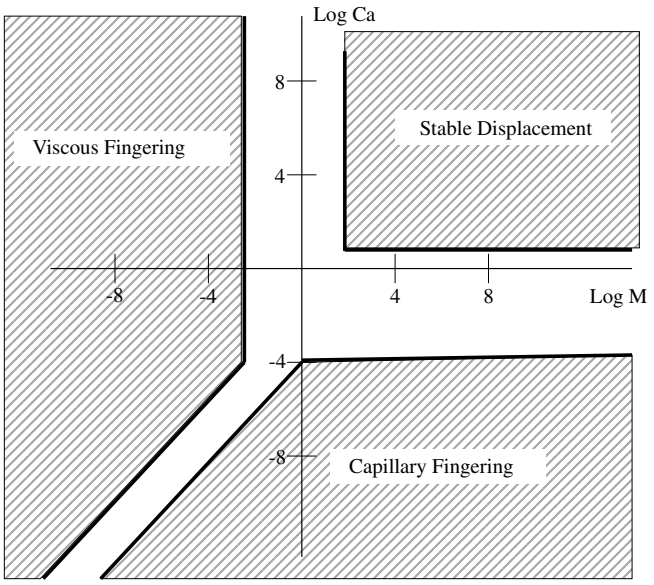

Fig. 5. Lenormand diagram.
Source: (After Lenormand et al., 1988.)

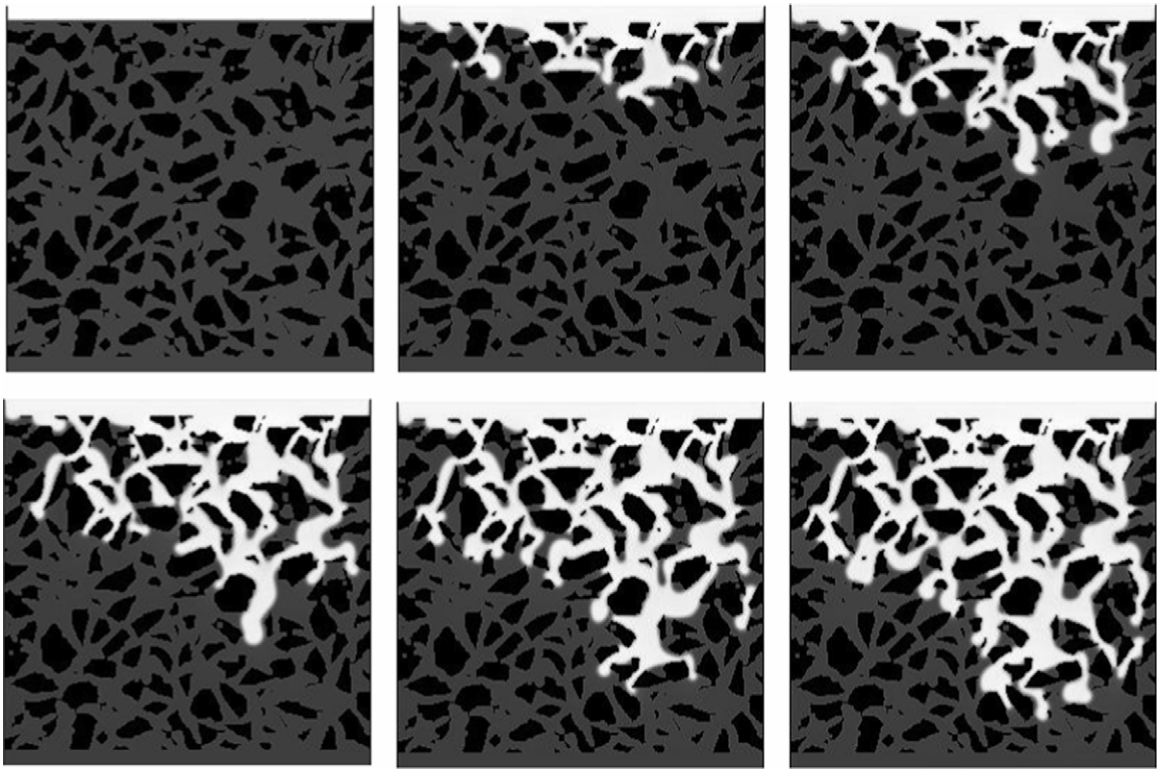

Fig. 6. Sequence of simulations of two-phase flow in a packed bed of sand particles. Percolation simulations by the single-component He–Chan–Zhang LBM. For a density ratio = 3.0 and $Ca = 6.77 \times 10^{-2}$. Lattice size 256×256 lu^2. Images are taken each 5000 iteration steps.

the image the affinity has been defined such that the contact angle is 45 degrees.

3.4. Simulation of fluid penetration and capillary phenomena in porous media

This section shows how the model proposed by He et al. and the proposed solid–fluid interaction explained before can be extended to the analysis and simulation of two-phase flow in complex porous structures. First, we show the behavior of the model in simple capillary tubes and later we extend the model for simulation of percolation in real 3D images of a captured porous structure with X-ray microtomography (XMT).

To drive the flow in these simulations, the Zuo and He method [31] has been used to define the pressure boundary condition along the flow direction. This method allows setting the exact pressure difference between the inlet and outlet as is the usual practice in standard Navier–Stokes solvers.

In a capillary tube, there is fluid displacement when the flow is driven by a difference in pressure strong enough to overcome the capillary pressure. Fig. 4 shows images of a capillary tube where the non-wetting fluid displaces the wetting fluid (drainage process) from left to right. In this case, we have taken the simplest case of two-phase flow of two porous channels of different diameter under the same pressure difference. As Fig. 4 shows, one of the throats is six times smaller than the other and therefore it has a six times higher entry pressure. The pressure across the phases has been set in such a way that the value is higher than the entry pressure for the bigger diameter throat but smaller than the entry pressure for the smaller diameter throat. Fig. 4 shows a sequence of images from left to right and top to bottom. In this sequence it is possible to observe the preferential flow that is developed by the meniscus which invades the channel with the higher throat radius having a smaller flow resistance. In conclusion, it is evident that this modified He–Chen–Zhang model has a good qualitative agreement with theory for two-phase flow in porous media, and in what follows we proceed to its application to real porous networks.

Lenormand et al. [32] ran numerous network simulations and performed experiments in transparent etched networks to identify patterns and describe the percolation of a non-wetting fluid when injected into a medium saturated with a wetting fluid. As an outcome of his research, he proposed a phase diagram for immiscible displacement characterized by the capillary number (Ca) and the viscosity ratio (M), as shown in Fig. 5. The diagram shows the existence of three basic domains of fluid penetration: stable displacement, viscous fingering, and capillary fingering.

In the stable displacement region, the major force is due to viscosity interaction of the injected fluid. The flow shows a flat front moving towards the exit with some irregularities on the size of a few pore scales.

In the viscous fingering region, the major force is due to viscosity interaction of the displaced fluid. In this type of flow the fingers look like a tree with no loops, and they spread across the porous network growing towards the exit.

In the capillary fingering region, the major force is due to capillarity, which also exhibits three-like fingering, but the fingers grow in all directions, even toward the entrance, forming loops. These loops trap the displaced wetting fluid leading to a higher final saturation than the viscous fingering.

Fig. 6 shows simulations of the interface advance by using the He–Chen–Zhang model applied to a packed bed of sand particles where the pore network has been captured by XMT analysis. The flow goes from top to bottom and is induced with a fixed pressure difference. The parameters of the simulation in Fig. 6 are set in such a way to obtain a flow in the transition zone between capillary fingering and stable displacement as described by Lenormand. The capillary number is only 6.77×10^{-2} and the density ratio is 3.

As can be seen in the sequence of images, the simulation starts from complete saturation of the wetting phase which is

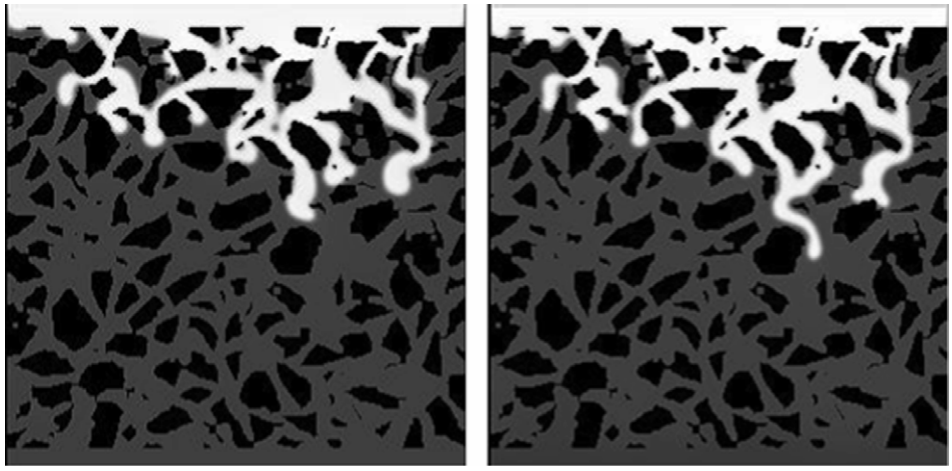

Fig. 7. Two different penetration simulations for the same density ratio (3.0) and pressure gradient but different surface tension. The left image has a high surface tension ($\bar{k} = 0.1$, $Ca = 6.77 \times 10^{-2}$) and the right image has a low surface tension ($\bar{k} = 10^{-5}$, $Ca = 230$). Both images were taken after 10 000 iterations.

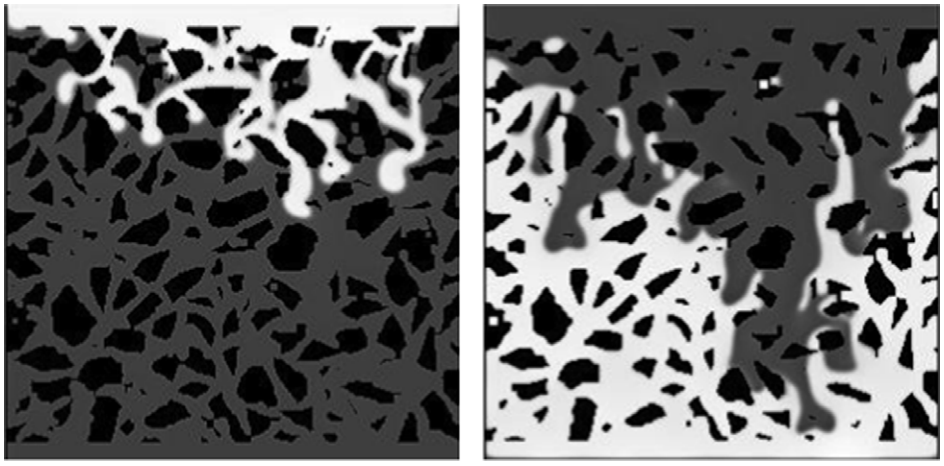

Fig. 8. Two different penetration simulations for the same surface tension but inverse density ratio. The left image has a density ratio = 3/1 and $Ca = 6.77 \times 10^{-2}$. The right image has a density ratio = 1/3 and $Ca = 1.32 \times 10^{-1}$. Both images were taken after 10 000 iterations.

displaced by a non-wetting phase. In the course of simulation the flow goes through the less resistant paths (coarser diameter pores) leaving behind some residual wetting phase trapped in very small pore spaces which have a high flow resistance and where the non-wetting phase cannot enter until the pressure increases. In agreement with the diagram proposed by Lenormand, and even though we are working at a pore scale level, the pattern of percolation shows a capillary fingering type of flow with relatively short fingers.

Fig. 7 shows a comparison of the same simulation shown in Fig. 6 against a new simulation where the surface tension has been reduced. Comparison at the same level of iteration shows that the percolation follows the same pattern for both multiphase flow in porous media simulations in this porous network structure, probably due to the fact that both simulations are run with the same pressure gradient and therefore the path of least resistance has not changed; however, the reduction of the surface tension produces longer and thinner fingers.

Fig. 8 shows a comparison between the same simulations of Fig. 6 against one simulation where the density ratio has been inverted. In this new case, the low density fluid displaces the heavier fluid and the pattern of flow changes since the pressure field has changed. According to the Lenormand diagram a stronger viscous fingering type of flow is expected to be observed with more and longer fingers being formed due to the stronger viscous interaction and interface front instability. As the comparison in Fig. 8 shows, there is a clear qualitative agreement between theory and simulations. Fingers are formed in zones of low resistance to flow, and once formed they start growing rapidly towards the exit.

Even though the He–Chen–Zhang model has advantages over other methods, such as its thermodynamic consistency, which makes the treatment of the surface tension easier because it can be set before actually running the simulation, on the other hand, it has the problem that it has not been extended to more than one-component simulation, and therefore two-phase flow is a mathematical artifact where both fluid phases are related by an equation of state. This characteristic imposes some restrictions, such as under certain pressure changes and flow conditions unexpected condensation and evaporation of the phases can be induced.

Although the use of an equation of state to induce phase segregation is a simple an elegant formulation for interfacial dynamic simulation, it restricts the one-component simulation to industrial applications for the simulations of liquid–vapor phase systems like water–water-vapor. However, the simulations can be of great importance in qualitative analysis for a better understanding of complex multiphase problems if we use the concept of dynamic similitude for fluid flow conditions and if the condensation/evaporation effect can be assumed to be negligible.

4. Summary

We have been successful in implementing the 2D and 3D software capabilities of lattice Boltzmann simulation for

multiphase fluid flow in porous media. The single-component multiphase flow He–Chen–Zhang LBM model has been extended to incorporate fluid–solid interaction forces and has been applied to the simulation of percolation in actual XMT images of pore network structures created by packed particle beds. Finally, in order to evaluate the actual potential of this mathematical model to simulate real multiphase problems, a comparison between experimental data and simulation results is in progress with respect to the relative permeability curves of a oil-well core sample, and the results will be presented in a separate paper. This is a particularly challenging problem because of the complexity of the physical phenomena involved and the size of the computing resources required.

Acknowledgements

Our special thanks are given to the Institute of Clean and Secure Energy (ICSE) at the University of Utah for their financial support.

References

[1] Zhang DF, Stone HA. Drop formation in viscous flows at a vertical capillary tube. Phys Fluids 1997;9:2234–42.
[2] Unverdi SO, Tryggvason G. A front-tracking method for viscous, incompressible multi-fluid flows. J Comput Phys 1992;100:25–37.
[3] Shyy W, Udaykumar HS, Madhukar MR, Smith RW. Computational fluid dynamics with moving boundaries. Mineola (NY): Dover Publications, Inc.; 1996.
[4] Cho Z, Jones J, Singh M. Foundations of medical imaging. New York: John Wiley & Sons; 1998.
[5] Rothman DH, Zaleski S. Lattice-gas models of phase separation: interfaces, phase transitions, and multiphase flow. Rev Modern Phys 1991;66:1417–79.
[6] Langaas K, Papatzacos P. Numerical investigations of the steady state relative permeability of a simplified porous medium. Transp Porous Media 2001;45:241–66.
[7] Kang Q, Zhang D, Chen S. Immiscible displacement in a channel: simulations of fingering in two dimensions. Adv Water Res 2004;27:13–22.
[8] Thies M. Lattice Boltzmann modeling with free surfaces applied to formation of metal foams. PhD. Thesis, Der Technischen Fakultät der Universität Erlangen-Nürnberg zur Erlangung des Grades, Erlangen, Germany. 2005. p. 177.
[9] Shan X, Chen H. Lattice Boltzmann model for simulating flows with multiple phases and components. Phys Rev E 1993;47:1815–9.
[10] Shan X, Chen H. Simulation of nonideal gases and liquid–gas phase transitions by the lattice Boltzmann equations. Phys Rev E 1994;49:2941–8.
[11] Shan X, Doolen G. Multicomponent lattice-Boltzmann model with interparticle interaction. J Stat Phys 1995;81:379–93.
[12] Shan X, Doolen G. Diffusion in a multicomponent lattice Boltzmann equation model. Phys Rev E 1996;54:3614–20.
[13] Swift MR, Osborn WR, Yeomans JM. Lattice Boltzmann simulation of nonideal fluids. Phys Rev Lett 1995;75:830–3.
[14] Swift MR, Orlandini E, Osborn WR, Yeomans JM. Lattice Boltzmann simulations of liquid–gas and binary fluid systems. Phys Rev E 1996;54:5041–52.
[15] Rothman DH, Keller JM. Immiscible cellular-automaton fluids. J Stat Phys 1988;52:1119–27.
[16] Gunstensen AK, Rothman DH, Zaleski S, Zanetti G. Lattice Boltzmann model of immiscible fluids. Phys Rev E 1991;43:4320–7.
[17] Grunau D, Chen S, Eggert K. A lattice Boltzmann model for multiphase fluid flows. Phys Fluids A 1993;5:2557–62.
[18] Chen S, Doolen G. Lattice Boltzmann method for fluid flows. Annu Rev Fluid Mech 1998;30:329–64.
[19] Do-Quang M, Aurell E, Vergassola M. An inventory of lattice Boltzmann models of multiphase flows. Parallel and Scientific Computing, Report 00:03, Royal Institute of Technology and Uppsala University. 2000.
[20] He X, Doolen G. Thermodynamics foundations of kinetic theory and lattice Boltzmann models for multiphase flow. J Stat Phys 2002;107:309–28.
[21] Házi G, Imre A, Mayer G, Farkas I. Lattice Boltzmann methods for two-phase flow modelling. Ann Nuclear Energy 2002;29:1421–53.
[22] Nourgaliev RR, Dinh TN, Theofanous TG, Joseph D. The lattice Boltzmann equation method: theoretical interpretation, numerics and implications. Int J Multiph Flow 2003;29:117–69.
[23] He X, Chen S, Zhang R. A lattice Boltzmann scheme for incompressible multiphase flow and its applications in simulation of Rayleigh–Taylor instability. J Comput Phys 1999;152:642–63.
[24] He X, Zhang R, Chen S, Doolen G. On the three-dimensional Rayleigh–Taylor instability. Phys Fluid 1999;11:1143–52.
[25] He X, Shan X, Doolen G. Discrete Boltzmann equation model for nonideal gases. Phys Rev E 1998;57:R13–6.
[26] Zhang R, He X, Chen H. Interface and surface tension in incompressible lattice Boltzmann multiphase model. Comput Phys Comm 2000;129:121–30.
[27] Lee T, Lin C. A stable discretization of the lattice Boltzmann equation for simulation of incompressible two-phase flows at high density ratio. J Comput Phys 2005;206:16–47.
[28] Waddell JT, Niederhaus CE, Jacobs JW. Experimental study of Rayleigh–Taylor instability: low Atwood number liquid systems with single-mode initial perturbations. Phys Fluids 2001;13:1263–73.
[29] Rothman DH, Zaleski S. Lattice-gas cellular automata. Cambridge University Press; 1997. p. 320.
[30] Yiotis AG, Psihogios J, Kainourgiakis ME, Papaioannou A, Stubos AK. A lattice Boltzmann study of viscous coupling effects in immiscible two-phase flow in porous media. Colloids Surf A 2007;300:35–49.
[31] Zuo Q, He X. On pressure and velocity boundary conditions for the lattice Boltzmann BGK model. Phys Fluids 1997;9:1591–8.
[32] Lenormand R, Touboul E, Zarcone C. Numerical methods and experiments on immiscible displacements in porous media. J Fluid Mech 1988;189:165–87.